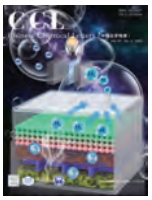
Chinese Chemical Letters 37 (2026) 111215

Contents lists available at ScienceDirect

Chinese Chemical Letters

journal homepage: www.elsevier.com/locate/cclet



High efficiency detection of Zn^{2+} through the improved electron density of aromatic π-conjugated bridges

Xindi Yang[a,b,1], Cunli Wang[b,1,*], Dongdong Wang[b,1], Haijuan Qin[c,1], Kuoxi Xu[a,1,*], Guangyan Qing[b,1,*]

[a] Henan Engineering Research Center of Industrial Recirculating Water Treatment, College of Chemistry and Molecular Sciences, Henan University, Kaifeng 475004, China
[b] CAS Key Laboratory of Separation Science for Analytical Chemistry, Dalian Institute of Chemical Physics, Chinese Academy of Sciences, Dalian 116023, China
[c] Research Centre of Modern Analytical Technology, Tianjin University of Science and Technology, Tianjin 300457, China

ARTICLE INFO

Article history:
Received 15 January 2025
Revised 8 April 2025
Accepted 15 April 2025
Available online 17 April 2025

Keywords:
Zn^{2+}
Fluorescent probe
π-Conjugated bridge
Near-infrared
Large Stokes shift
High selectivity

ABSTRACT

Zinc ions (Zn^{2+}) play a crucial role in maintaining human health, and their imbalance has been associated with various diseases and environmental contamination. Although many fluorescent probes have been developed for Zn^{2+} detection, they often face challenges, including short emission wavelengths, narrow Stokes shifts, and particularly the poor selectivity. Here, aromatic rings with different electron densities including benzene, thiophene and furan rings, were introduced as aromatic π-conjugated bridges to connect dicyanoisophorone (DCI) and amide-di-2-picolylamine (DPA) based structures, and three probes **L1**, **L2** and **L3** for Zn^{2+} detection were developed. Our results demonstrated that compared with **L1**, **L2** and **L3**, which inserting thiophene and furan rings, revealed near-infrared (NIR) emission at 651 nm, and a larger Stokes shift of 187 nm. Notably, different from **L2**, **L3**, which incorporated a furan ring with the highest electron density, exhibited the highest selectivity for Zn^{2+} with a low detection limit of 31 nmol/L. In addition, the binding mode of **L3** with Zn^{2+} was confirmed in the form of an imidic acid tautomer. Furthermore, **L3** was successfully applied in cellular imaging, validating its potential for *in vivo* bioimaging. This study presents a promising strategy for developing high-performance Zn^{2+} probes by simply modifying the aromatic π-conjugated bridges.

© 2026 Published by Elsevier B.V. on behalf of Chinese Chemical Society and Institute of Materia Medica, Chinese Academy of Medical Sciences.

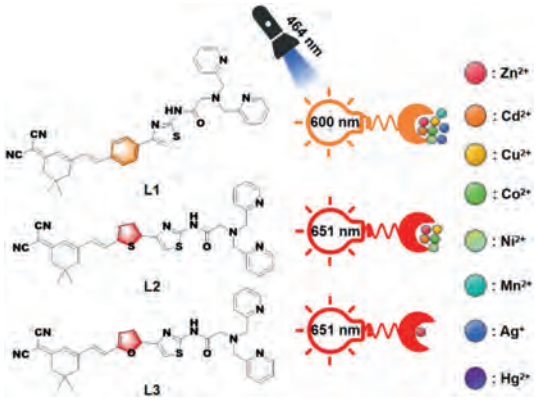
Zinc ions (Zn^{2+}) play important roles in various biological processes in the human body [1]. For instance, Zn^{2+} is a co-factor for various physiological responses, including gene expression, apoptosis, neurotransmission, enzyme regulation, and metabolic function [2–4]. The extent of Zn^{2+} deficiency is also associated with physical growth retardation and neurological disorders, such as Alzheimer's disease [5–7], Parkinson's disease [8,9], and depression [10,11]. In modern industry, Zn^{2+} pollution in soil and water has become a widespread problem [12–14].

To date, several methods including fluorescent probes [15], electrochemical methods [16], atomic absorption spectrometry [17], atomic emission spectrometry [18], and mass spectrometry [19], have been developed for Zn^{2+} analysis. Compared to other methods, fluorescent probes have emerged as a promising tool for detecting Zn^{2+} due to their low cost, high sensitivity, and real-time detection capability [20,21]. Numerous fluorescent probes for Zn^{2+} detection have been developed, however, they have some limitations such as short emission wavelengths, narrow Stokes shifts, and the poor selectivity, which limit their practical applications [22–27]. Therefore, developing Zn^{2+} fluorescent probes that can avoid these limitations is of great significance.

A typical fluorescent probe for metal ion recognition must contain a receptor (the recognition site) linked to a fluorophore (the signal source), which translates the recognition event into the fluorescence signal [28]. Among various fluorophores, dicyanoisophorone (DCI) based fluorophores have the advantage of near-infrared (NIR) emission, a large Stokes shift, and excellent photostability, making it one of the most popular signal groups for fluorescent probes [29–32]. To achieve longer emission wavelengths and larger Stokes shifts based on DCI, an effective approach is to increase the electron density of π-conjugated linkers (π-conjugated bridge) linked with DCI [33–35]. However, achieving excellent ion selectivity of the fluorescent probes for metal ions,

* Corresponding authors.
E-mail addresses: wangcunli@dicp.ac.cn (C. Wang), xukx@henu.edu.cn (K. Xu), qinggy@dicp.ac.cn (G. Qing).
[1] These authors contributed equally to this work.

https://doi.org/10.1016/j.cclet.2025.111215
1001-8417/© 2026 Published by Elsevier B.V. on behalf of Chinese Chemical Society and Institute of Materia Medica, Chinese Academy of Medical Sciences.



Scheme 1. The structure of **L1**, **L2** and **L3**, and their selectivity for Zn^{2+} detection.

especially Zn^{2+}, remains a critical challenge [22,26,27]. The receptor, which serves as the central processing unit of the probe, must exhibit the strongest affinity with Zn^{2+}. Di-2-picolylamine (DPA) unit is commonly used for Zn^{2+} detection, but it also has similar affinities for other transition metal ions such as Co^{2+}, Ni^{2+}, Cu^{2+}, Cd^{2+}, and Hg^{2+} [36]. Commonly, Zn^{2+} selectivity can be enhanced by optimizing the DPA structure [37]. Xu *et al.* reported a probe named ZTRS for Zn^{2+} detection, which was comprised of amide-DPA receptor and a naphthalimide fluorophore. Consequently, ZTRS showed excellent selectivity for Zn^{2+} over other transition metal ions [38]. Liu *et al.* introduced the amide-DPA receptor to a nitrobenzofurazan fluorophore, and this probe displayed unexpected high selectivity for Cd^{2+} rather than Zn^{2+} [39]. These findings suggest that a probe containing a specialized fluorophore with an amide-DPA-based receptor may achieve the desired selectivity for Zn^{2+}. As mentioned above, we aimed to improve the electron density of the π-conjugated bridge to achieve longer emission wavelengths and larger Stokes shifts in the DCI-based fluorophore. However, it remains unclear whether this modification will improve the ion selectivity of the amide-DPA based receptor for Zn^{2+}.

We addressed the issues here. In this study, various aromatic rings, including benzene, thiophene, and furan rings, are selected as the aromatic π-conjugated bridges. Additionally, thiazole, a widely recognized biocompatible structural unit, is used to modify the amide-DPA receptor to reduce the toxicity of the whole fluorescent probe [40–42]. As shown in Scheme 1, the structures of three fluorescent probes (abbreviated as **L1**, **L2**, **L3**) are presented. Among the three probes, **L1**, containing the benzene ring with the lowest electron density, exhibited the shortest emission wavelength (600 nm) and poorest ion selectivity. In contrast, **L2** and **L3** with higher electron density bridges (thiophene and furan, respectively) demonstrated red-shifted emission at 651 nm with a large Stokes shift of 187 nm, and enhanced Zn^{2+} selectivity. Notably, probe **L3**, which incorporates a furan ring (exhibiting the highest electron density among the three aromatic systems investigated), achieved optimal performance, demonstrating superior Zn^{2+} selectivity with a detection limit of 31 nmol/L. In addition, we demonstrated the binding mode of **L3** with Zn^{2+}. Furthermore, fluorescence images demonstrated the outstanding capability of **L3** for Zn^{2+} cellular imaging. Importantly, we developed a smart strategy by regulating the electron density of the aromatic π-conjugated bridge to improve the Zn^{2+} selectivity of the probe, which could be expected to apply to various metal ions detection in future.

L1, **L2** and **L3** were synthesized following Scheme S1 (Supporting information), and all the structures were confirmed by ^{1}H nuclear magnetic resonance spectra (NMR), ^{13}C NMR, and mass spectrometry (MS) (Figs. S1–S29 in Supporting information). The molecular formulas of **L1**, **L2** and **L3** were shown in Scheme 1.

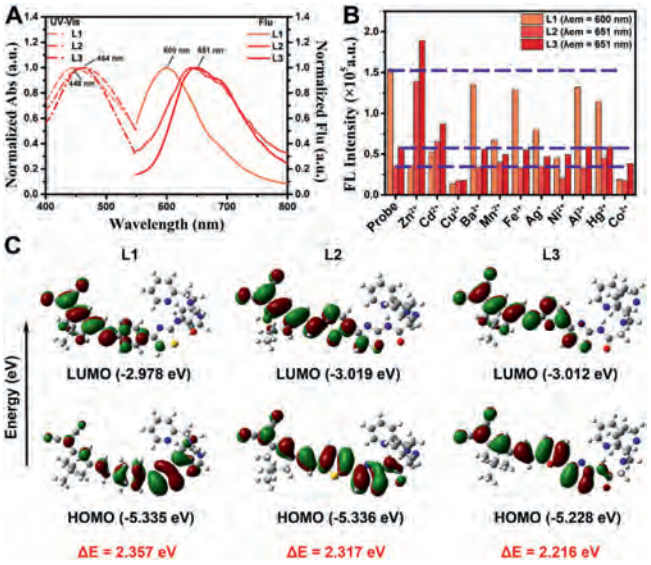


Fig. 1. (A) UV–vis and fluorescence spectra of **L1**, **L2** and **L3** (3.33×10^{-5} mol/L) in a DMSO/Tris–HCl buffer solution (v:v = 1:2, 0.01 mol/L, pH 7.30) at room temperature. Spectra were normalized to the maximum emission intensity of each probe. (B) Fluorescence intensity of **L1**, **L2** and **L3** upon the addition of various metal ions (10.0 equiv.) in a DMSO/Tris–HCl buffer solution (v:v = 1:2, 0.01 mol/L, pH 7.30) at room temperature. The excitation wavelength (λ_{ex}) was 464 nm for all the fluorescence measurements. (C) HOMO, LUMO, and band gap energies $-\Delta E = E_{HOMO} - E_{LUMO}$ of **L1**, **L2** and **L3** obtained through the TDDFT calculation.

Initially, we measured the UV–vis and fluorescence spectra of **L1**, **L2**, and **L3** (Fig. 1A) and evaluated their selectivity toward metal ions through fluorescence spectra experiment (Fig. 1B and Fig. S30 in Supporting information). As shown in Fig. 1A, the emission wavelength of **L1** was observed at 600 nm, with a Stokes shift of 152 nm. In Fig. 1B, the fluorescence intensity at 600 nm of **L1** was quenched obviously after the stock solutions of Zn^{2+}, Cd^{2+}, Ag^{+}, Ni^{2+}, Co^{2+}, Hg^{2+}, Cu^{2+} and Mn^{2+} treatment, indicating the poor selectivity of **L1**. Due to the unsatisfactory performance of **L1**, we aimed to enhance the electron density of the aromatic π-conjugated bridge to achieve longer emission wavelengths and higher metal ion selectivity. It is well known that thiophene ring has a higher electron density than the benzene ring, and thus it was applied in this event [35,43]. As anticipated, compared with **L1**, **L2** exhibited a NIR emission wavelength at 651 nm and an increased Stokes shift raising from 152 nm to 187 nm (Fig. 1A). And the metal ion selectivity of **L2** for Zn^{2+} was improved a lot as indicated by the fluorescence intensity increased 4 times upon the addition of Zn^{2+} (Fig. 1B). However, Cu^{2+}, Ni^{2+}, and Co^{2+} were found to quench the fluorescence of **L2**. Based on this, in order to further enhance Zn^{2+} selectivity, we replaced the benzene ring with a furan ring, which has an even higher electron density [35]. As a result, **L3** showed the same NIR emission and large Stokes shift as **L2** (Fig. 1A). Astonishingly, the selectivity of **L3** for Zn^{2+} was significantly improved showed by the fluorescence intensity increased 3 times (Fig. 1B). Among the eleven metal ions investigated, Cu^{2+} exhibited exclusive capability to induce complete fluorescence quenching of **L3**, demonstrated by a significant decrease in fluorescence intensity at 651 nm.

To better understand the relationship between molecular structure and the photophysical properties, time-dependent density functional theory (TDDFT) calculations were performed to calculate the highest occupied molecular orbital (HOMO) and the lowest unoccupied molecular orbital (LUMO) [44]. As shown in Fig. 1C, the band gap energies (ΔE) of **L2** and **L3** were 2.317 and 2.216 eV, respectively, which is smaller than that of **L1** (2.357 eV). As previously reported, a reduced bandgap results in a red-shift in the

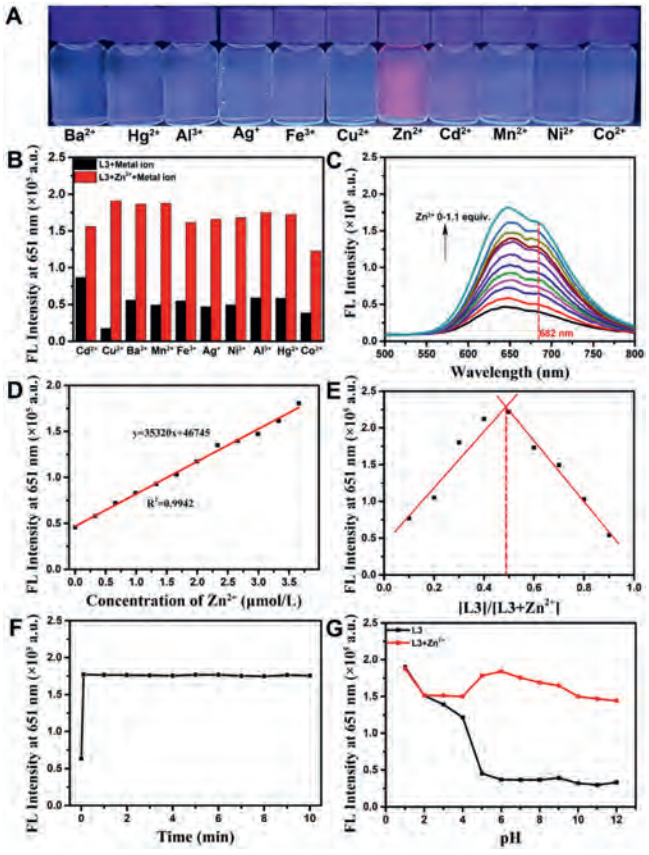


Fig. 2. (A) Photo of **L3** (3.33×10^{-5} mol/L) upon the addition of different metal ions (10.0 equiv.) in a DMSO/Tris–HCl buffer solution (v:v = 1:2, 0.01 mol/L, pH 7.30) at room temperature, excited with an UV–vis light (365 nm). (B) Fluorescence intensity (at 651 nm) of **L3** solution with the addition of different metal ions (10.0 equiv.) in the absence (black) and presence (red) of 10.0 equiv. of Zn^{2+}. (C) Fluorescence spectra and (D) fluorescence intensity changes (at 651 nm) of **L3** upon the addition of different equiv. of Zn^{2+} (0–1.1 equiv.). (E) Job's plot for determining the binding stoichiometry between **L3** and Zn^{2+} in the buffer solution based on the fluorescence intensity changes at 651 nm. (F) Time and (G) pH dependence of fluorescence intensity (at 651 nm) of **L3** upon the addition of 10.0 equiv. of Zn^{2+}. The excitation wavelength (λ_{ex}) was 464 nm for (B–G).

optical range [45,46]. This outcome demonstrates that enhancing the electron density of aromatic π-conjugated bridges effectively amplifies both the extended emission wavelengths and the larger Stokes shifts. Additionally, the HOMO of these probes is primarily delocalized over the DCI-π-conjugated bridge-thiazole, while the LUMO is largely confined to the DCI and π-conjugated bridge, leading to charge separation (Fig. 1C). In the case of **L1** containing a benzene bridge, the HOMO distribution across the DCI-π-conjugated bridge is relatively localized. In contrast, **L2** and **L3**, featuring thiophene and furan bridges respectively, demonstrate enhanced electron delocalization within their π-conjugated bridge systems. This suggests that the strategy of increasing electron density in aromatic π-conjugated bridges enhances HOMO-LUMO orbital overlap through improved electron delocalization. Collectively, aromatic π-conjugated bridges with higher electron density synergistically promote frontier molecular orbital (FMO) overlap and reduce the bandgap, thereby facilitating intramolecular charge transfer and triggering a selective fluorescent response of the probe toward Zn^{2+} [35,47,48].

Owing to the strong emission of **L3** in the NIR region when combined with Zn^{2+}, the fluorescence could be directly observed by naked eyes. Fig. 2A depicted a photo of **L3** solutions containing various metal ions (10.0 equiv.) including Zn^{2+}, Ba^{2+}, Hg^{2+}, Al^{3+}, Ag^{+}, Fe^{3+}, Cu^{2+}, Cd^{2+}, Mn^{2+}, Ni^{2+} and Co^{2+} through the UV–vis light. After being irradiated by a bright light with a single wavelength of 365 nm, only the solution with Zn^{2+} emitted strong red fluorescence, highlighting the exceptional specificity of **L3** for Zn^{2+}. To further investigate its ability to recognize Zn^{2+} in various interference, a series of competitive experiments were performed in the presence of the above metal ions. As shown in Fig. 2B, first, 10.0 equiv. of other metal ions were added to a series of **L3** solutions (3.33×10^{-5} mol/L), and no evident changes in the fluorescence intensity were observed for these metal ions (blank columns). Then, 10.0 equiv. of Zn^{2+} was added to these mixtures, and all the fluorescence intensity of **L3** sharply increased from approximately 0.5×10^5 to 1.7×10^5 (red columns), which indicated that **L3** could specifically bind to Zn^{2+} even under the strong interference of other metal ions. To determine the limit of detection (LOD), varying amounts (0–1.1 equiv.) of Zn^{2+} were added to **L3** solution and the fluorescence intensity was recorded (Fig. 2C). Fig. 2D showed a linear relationship between the fluorescence intensity at 651 nm and the concentration of Zn^{2+} ranging from 0 to 3.66×10^{-5} mol/L. And the LOD was determined to be 31 nmol/L [49]. In addition, to ascertain the stoichiometry of **L3** and Zn^{2+}, a Job's plot was conducted [50]. Shown as in Fig. 2E, the maximum change in the fluorescence intensity ($I_0 - I$) was found to be at about 0.5 of the molar fraction ([**L3**]/[**L3**+Zn^{2+}]), suggesting a 1:1 coordinative stoichiometry. The formation of a 1:1 complex was further confirmed by high-resolution mass spectrometry (HRMS), with a distinct peak at *m/z* 664.1365 corresponding to [**L3**+Zn^{2+}−H^{+}]$^{+}$ (calcd. *m/z* 664.1468) (Fig. S31 in Supporting information). As shown in Fig. 2F, time-dependent fluorescence changes at 651 nm indicated that **L3** responded rapidly to Zn^{2+}, suggesting its potential as an effective probe for real-time monitoring of Zn^{2+}. To expand the applicability of **L3** across a wide pH range, the fluorescence response of **L3** to Zn^{2+} was examined at pH values ranging from 1 to 12. In the pH range of 5–12, **L3** alone displayed weak fluorescence but showed a dramatic enhancement upon the addition of Zn^{2+}, indicating its ability to detect Zn^{2+} in a variety of physiological and basic environments. However, **L3** displayed strong fluorescence at more acidic conditions (pH < 5), and the further addition of Zn^{2+} did not result in further improvement (Fig. 2G). This pH-dependent fluorescence changes at low pH may be attributed to the inhibited photoinduced electron transfer (PET) process by protonation of the tertiary amine in DPA [38]. To further verify the stability of **L3**, we measured **L3**'s fluorescence spectra in different solvents (including DMSO, DMF, MeCN, THF, MeOH, EtOH, Tris, EAC, 1,4-dioxane, DCM and PE) and at varying temperatures (ranging from 10 °C to 60 °C). As shown in Fig. S32A (Supporting information), **L3** exhibited stable luminescent properties across various solvents. Additionally, the negligible changes in fluorescence spectra observed at different temperatures further confirm **L3**'s excellent stability (Fig. S32B in Supporting information).

As mentioned above, we have measured the changes of the fluorescence spectra of **L3** upon the addition of 10.0 equiv. of Zn^{2+} in DMSO/Tris–HCl buffer solution, and demonstrated that the fluorescence intensity increased at 651 and 682 nm (Fig. 2C). The same phenomenon was observed when the buffer solution changed into DMSO (Fig. S33 in Supporting information), which proved that the binding mode of **L3** with Zn^{2+} in the DMSO/Tris–HCl buffer solution was similar to that in DMSO. We proposed that the emission spectra observed in DMSO resulted from the transformable ability of **L3**, where Zn^{2+} induced a transformation of chelation from an amide to an imidic acid tautomeric form (Fig. 3A). To confirm this form with Zn^{2+}, we conducted ^{1}H NMR experiments of **L3** in the presence and absence of Zn^{2+} in DMSO–d_6. As depicted in Fig. 3B, the resonances of protons H8-H13 experienced down-field shifts upon the addition of 1.0 equiv. of Zn^{2+}, indicating the coordination of Zn^{2+} with the two pyridyl nitrogen atoms and the aliphatic amine nitrogen atom. In addition, the amide moiety binding to

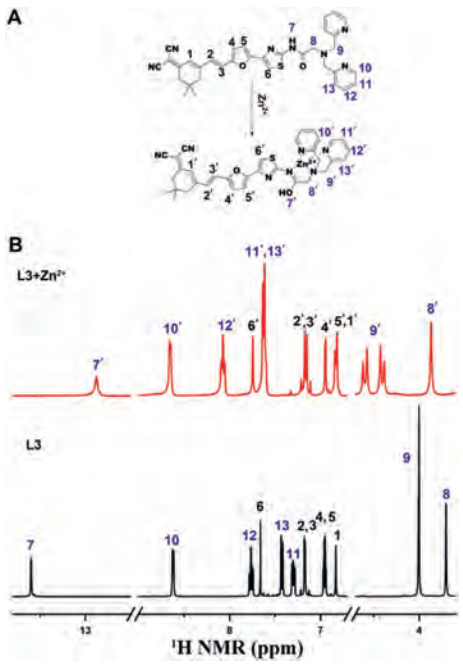


Fig. 3. (A) Binding mode of **L3** with Zn^{2+}. (B) ^1H NMR spectra of **L3** alone or in the presence of Zn^{2+} (1.0 equiv., red) in DMSO–d_6.

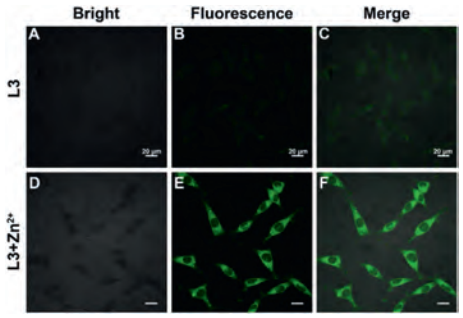


Fig. 4. (A, D) Bright field images, (B, E) LSCM fluorescence images, and (C, F) merged images of SHSY5Y cells. (A–C) Cells were treated with **L3** (10 μmol/L) for 30 min. (D–F) Cells were treated with Zn^{2+} (10 μmol/L) for 30 min following **L3** treatment. Laser Wavelength: 488 nm.

Zn^{2+} resulted in a small up-field shift of H7 from 13.60 ppm to 12.88 ppm, suggesting the formation of an imidic acid tautomeric [38]. Therefore, we proposed that **L3** binding to Zn^{2+} was also in an imidic acid tautomeric form in the DMSO/Tris–HCl buffer solution (Fig. 3A).

Compared with **L1** and **L2**, **L3** exhibited NIR emission, a large Stokes shift and superior anti-interference capability at physiological pH, rendering it an excellent probe for Zn^{2+} cellular imaging. Initially, we assessed the cytotoxicity of **L3** in SHSY5Y cells using the cell counting kit-8 (CCK-8) assay [51,52]. After SHSY5Y cells treated with different concentration of **L3** for 24 h, cell viability all remained above 80 %, indicating that **L3** possessed low cytotoxicity toward SHSY5Y cells (Fig. S34 in Supporting information). For Zn^{2+} cellular imaging, SHSY5Y cells were incubated with 10 μmol/L **L3** for 30 min at 37 °C and then washed three times with phosphate buffer saline (PBS). As depicted in Figs. 4A–C, the laser scanning confocal microscopy (LSCM) images revealed extremely weak fluorescence after treated with **L3** alone. Differently, a significant increase in fluorescence intensity was observed when cells were co-incubated with both **L3** and Zn^{2+} (Figs. 4D–F). The successful internalization of **L3** into SHSY5Y cells highlighted its biocompatibility and suitability for biological applications. The distinct fluorescence signal observed upon Zn^{2+} adding further confirmed the selectivity and sensitivity of **L3** toward Zn^{2+}.

In this study, we developed three fluorescent probes **L1**, **L2** and **L3**, and demonstrated that enhancing the electron density of the aromatic π-conjugated bridge can effectively improve the emission wavelength, Stokes shift, and ion selectivity of the probes. Among the three probes, **L3** achieved NIR emission at 651 nm, a Stokes shift of 187 nm, and superior Zn^{2+} selectivity with a detection limit of 31 nmol/L. And we also revealed that the amide of **L3** bound to Zn^{2+} was in the form of an imidic acid tautomer through fluorescence and ^1H NMR spectra. Furthermore, we successfully applied **L3** in live-cell Zn^{2+} imaging, demonstrating its potential to detect Zn^{2+} *in vivo*. This discovery provides valuable insights for optimizing probe performance through the simple introduction of the aromatic π-conjugated bridge.

Declaration of competing interest

The authors declare that they have no known competing financial interests or personal relationships that could have appeared to influence the work reported in this paper.

CRediT authorship contribution statement

Xindi Yang: Writing – original draft, Software, Methodology, Formal analysis, Data curation. **Cunli Wang:** Writing – review & editing, Writing – original draft, Validation, Supervision. **Dongdong Wang:** Software, Methodology, Formal analysis. **Haijuan Qin:** Formal analysis. **Kuoxi Xu:** Supervision, Resources, Project administration, Funding acquisition, Conceptualization. **Guangyan Qing:** Supervision, Resources, Project administration, Funding acquisition.

Acknowledgments

This work was supported by the National Key R&D Program of China (No. 2022YFC3400800), the National Natural Science Foundation of China (Nos. 21922411 and 22174138), DICP Innovation Funding (Nos. DICP-I202243 and I202229), and the Dalian Outstanding Young Scientific Talent (No. 2020RJ01).

Supplementary materials

Supplementary material associated with this article can be found in the online version, at doi:10.1016/j.cclet.2025.111215.

References

[1] C.J. Frederickson, J.Y. Koh, A.I. Bush, Nat. Rev. Neurosci. 6 (2005) 449–462.
[2] J.M. Berg, Y.G. Shi, Science 271 (1996) 1081–1085.
[3] H. Tapiero, K.D. Tew, Biomed. Pharmacother. 57 (2003) 399–411.
[4] B.L. Vallee, K.H. Falchuk, Physiol. Rev. 73 (1993) 79–118.
[5] J.H. Weiss, S.L. Sensi, J.Y. Koh, Trends Pharmacol. Sci. 21 (2000) 395–401.
[6] A.I. Bush, Trends Neurosci. 26 (2003) 207–214.
[7] P. Faller, C. Hureau, G.La Penna, Acc. Chem. Res. 47 (2014) 2252–2259.
[8] H. Kozlowski, M. Luczkowski, M. Remelli, D. Valensin, Coord. Chem. Rev. 256 (2012) 2129–2141.
[9] J.H. Viles, Coord. Chem. Rev. 256 (2012) 2271–2284.
[10] M. Siwek, B. Szewczyk, D. Dudek, et al., Pharmacol. Rep. 65 (2013) 1512–1518.
[11] M.T. Gong, Y.L. Fang, K.J. Yang, et al., Adv. Sci. 11 (2024) 2403405.
[12] C. Dewey, F. Juillot, S. Fendorf, J.R. Bargar, Environ. Sci. Technol. 57 (2023) 4841–4851.
[13] J. Helser, E. Vassilieva, V. Cappuyns, J. Hazard. Mater. 424 (2022) 127313.
[14] J. Xu, Y.Y. Li, S.L. Wang, et al., J. Hazard. Mater. 441 (2023) 129863.
[15] F. Wang, K.J. Wang, Q. Kong, et al., Coord. Chem. Rev. 429 (2021) 213636.
[16] R.Z. Ouyang, Z.Q. Zhu, C.E. Tatum, J.Q. Chambers, Z.L. Xue, J. Electroanal. Chem. 656 (2011) 78–84.
[17] K.K. Nielson, A.W. Mahoney, V.C. Rogers, J. Agric. Food Chem. 36 (1988) 1211–1216.
[18] S.V. Smirnova, T.O. Samarina, D.V. Ilin, I.V. Pletnev, Anal. Chem. 90 (2018) 6323–6331.
[19] H. Wang, B.B. Chen, M. He, B. Hu, Anal. Chem. 89 (2017) 4931–4938.
[20] Y.Y. Wang, H.N. Duan, H.Y. Shi, et al., Chin. Chem. Lett. 31 (2020) 2933–2936.

[21] S.A. Garwin, M.S. Kelley, A.C. Sue, et al., J. Am. Chem. Soc. 141 (2019) 16696–16705.
[22] L.Q. Yan, D.Q. Lu, H. Yang, X.Z. Wu, Spectrochim. Acta A: Mol. Biomol. Spectrosc. 290 (2023) 122243.
[23] F.J. Huo, Q. Wu, J. Kang, Y.B. Zhang, C.X. Yin, Sens. Actuators B: Chem. 262 (2018) 263–269.
[24] Z.Q. Mao, L. Hu, X.H. Dong, et al., Anal. Chem. 86 (2014) 6548–6554.
[25] W.Y. Li, B.Q. Fang, M. Jin, Y. Tian, Anal. Chem. 89 (2017) 2553–2560.
[26] H.N. Duan, Y. Ding, C.S. Huang, et al., Chin. Chem. Lett. 30 (2019) 55–57.
[27] X.D. Wei, Q. Wang, W.Q. Tang, S.L. Zhao, Y.S. Xie, Dyes Pigm. 140 (2017) 320–327.
[28] J.F. Callan, A.P. de Silva, D.C. Magri, Tetrahedron 61 (2005) 8551–8588.
[29] X.Z. Luo, F.F. Yu, R. Wang, et al., Chin. Chem. Lett. 36 (2025) 110531.
[30] L. Sheng, H.M. Liu, M. Jin, et al., Chin. Chem. Lett. 35 (2024) 109572.
[31] L.X. Dai, Q. Zhang, Q.Q. Ma, W.Y. Lin, Coord. Chem. Rev. 489 (2023) 215193.
[32] L.X. Fu, Y.Y. Tan, Y. Ding, W.X. Qing, Y. Wang, Chin. Chem. Lett. 35 (2024) 108886.
[33] W.Q. Chen, X.X. Yue, W.X. Li, et al., Sens. Actuators B: Chem. 245 (2017) 702–710.
[34] X. Luo, J. Li, J. Zhao, et al., Chin. Chem. Lett. 30 (2019) 839–846.
[35] H.W. Chen, H.W. Cao, J.Z. Li, et al., Spectrochim. Acta A: Mol. Biomol. Spectrosc. 323 (2024) 124901.
[36] B. Das, P. Gupta, Coord. Chem. Rev. 522 (2025) 216209.
[37] Z.C. Xu, J. Yoon, D.R. Spring, Chem. Soc. Rev. 39 (2010) 1996–2006.
[38] Z.C. Xu, K.H. Baek, H.N. Kim, et al., J. Am. Chem. Soc. 132 (2010) 601–610.
[39] Y. Liu, Q.L. Qiao, M. Zhao, et al., Dyes Pigm. 133 (2016) 339–344.
[40] H.B. Yang, H.T. Qi, Z.S. Hao, et al., Chin. Chem. Lett. 31 (2020) 1271–1275.
[41] M.T. Chhabria, S. Patel, P. Modi, P.S. Brahmkshatriya, Curr. Top. Med. Chem. 16 (2016) 2841–2862.
[42] A.K. Datusalia, G.L. Khatik, Curr. Drug Discov. Technol. 15 (2018) 162.
[43] R. Ali, R. Siddiqui, RSC Adv. 12 (2022) 36073–36102.
[44] S. Sumiya, Y. Shiraishi, T. Hirai, J. Phys. Chem. A 117 (2013) 1474–1482.
[45] S.D. Xu, Y.K. Duan, B. Liu, Adv. Mater. 32 (2020) 1903530.
[46] A. Ajayaghosh, Chem. Soc. Rev. 32 (2003) 181–191.
[47] H.H. Zhangsrt, C.X. Yan, H. Li, et al., ACS Appl. Bio Mater. 4 (2020) 2001–2008.
[48] T. Ye, M. Li, Y. Liu, Molecules 25 (2020) 4465.
[49] Y.X. Chang, H.J. Qin, X. Wang, et al., ACS Sens. 5 (2020) 2438–2447.
[50] F. Ulatowski, K. Dabrowa, T. Bałakier, J. Jurczak, J. Org. Chem. 81 (2016) 1746–1756.
[51] X.J. Zhao, X.Y. Chen, Y. Wu, et al., Spectrochim. Acta A: Mol. Biomol. Spectrosc. 309 (2024) 123806.
[52] C.Y. Li, X.K. Wang, X.F. Zhu, J.F. Liu, Y. Ye, Anal. Chim. Acta 1330 (2024) 343265.